International Journal of Thermophysics, Vol. 14, No. 3, 1993

Dielectric Function and Electrical Resistivity of Liquid Carbon Determined by Femtosecond Spectroscopy[1]

M. C. Downer,[2] H. Ahn,[2] D. H. Reitze,[2] and X. Y. Wang[2]

Femtosecond pump-probe reflectance of graphite and diamond targets following intense laser irradiation is used to measure the optical properties of the pressurized liquid carbon phase while it retains an optically sharp surface before expanding hydrodynamically as a hot plasma. These measurements allow the historically elusive liquid phase of carbon to be characterized optically for the first time. A Drude dielectric model of the reflectance spectrum 1 ps after excitation just above the melting threshold reveals a poorly conducting liquid metal with a dc resistivity $625 \pm 75\ \mu\Omega \cdot$ cm. The optically determined resistivity decreases with increasing sample excitation. The initial stages of hydrodynamic surface expansion of Al, W, and C targets are also quantitatively characterized by time-resolved reflectance, revealing the expansion speed as well as further dielectric properties of the high-temperature–pressure phase.

KEY WORDS: femtosecond spectroscopy; laser irradiation; liquid carbon; optical properties; reflectivity.

1. INTRODUCTION

Bench-scale femtosecond laser systems delivering light pulses up to 1-J energy [1–3] are opening a significant new direction in subsecond thermophysical measurements. In contrast to longer laser pulses, a femtosecond pulse deposits its energy in the target surface before significant hydrodynamic motion orthogonal to the surface occurs, as depicted in Fig. 1. The photoexcited region is thus not only strongly heated, but also

[1] Paper presented at the Third Workshop on Subsecond Thermophysics, September 17–18, 1992, Graz, Austria.

[2] Physics Department, University of Texas at Austin, Austin, Texas 78712, U.S.A.

0195-928X/93/0500-0361$07.00/0 © 1993 Plenum Publishing Corporation

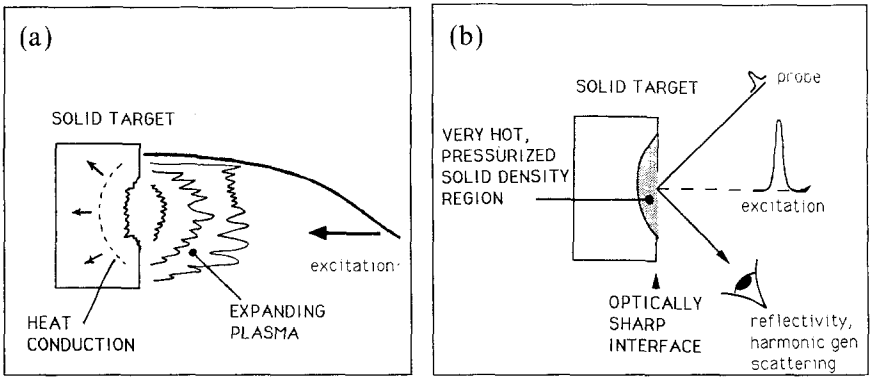

Fig. 1. Schematic diagram of solid target conditions immediately following intense optical excitation in two contrasting pulse width regimes. (a) With a long (>10-ps) light pulse, significant hydrodynamic expansion and heat conduction out of the absorption depth occur during excitation, leaving a complicated material density and temperature distribution. (b) With a femtosecond heating pulse, the fully heated surface retains an optically sharp interface for 1–2 ps, permitting precise spectroscopic characterization of the solid density fluid via surface reflectance methods with a time-delayed, tunable femtosecond probe pulse. After tens of picoseconds, the situation in b approaches conditions similar to those depicted in a.

pressurized into the Mbar regime because it is heated at constant volume, prior to thermal expansion. In addition, the hot pressurized region retains an optically sharp interface for several picoseconds, allowing adequate time for electron-lattice equilibration, melting, and precise optical characterization of the fluid by surface reflectance or nonlinear optics using a time-delayed femtosecond probe pulse. Historically, such optical measurements have provided an important key to the underlying electronic properties of condensed matter at low temperature and pressure. Femtosecond experiments extend traditional condensed matter spectroscopy to previously inaccessible pressure–temperature regimes and, therefore, complement traditional subsecond thermophysical measurements. They are analogous to studying optically polished samples of material from planetary and stellar interiors. Several recent studies used a single intense pulse serving as both excitation and optical probe [4–6]. Our experiments use time-resolved pump-probe methods to elucidate the competing processes of electron heating, melting, and hydrodynamic surface expansion, which influence surface reflectance to different degrees and at different times.

2. FEMTOSECOND HUGONIOT

Figure 2a depicts the Hugoniot corresponding to constant volume heating of a carbon target, superimposed on the equilibrium phase diagram

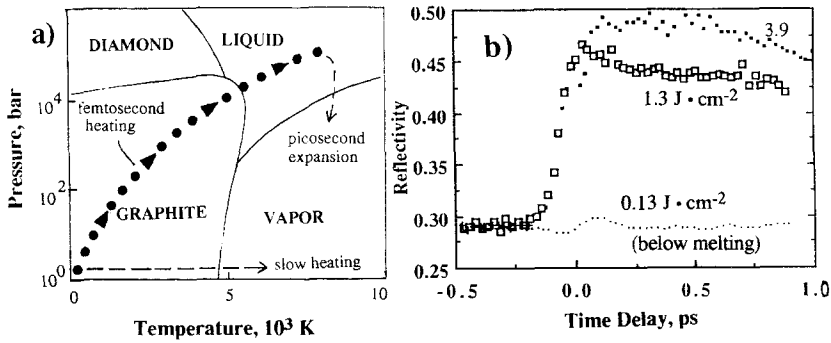

Fig. 2. (a) Equilibrium phase diagram of carbon in pressure and temperature regimes accessible in pulsed laser heating experiments. Slow pulsed heating leads to little change in sample pressure, since thermal expansion can occur during the pulse. Femtosecond heating creates substantial internal pressure, allowing temporary access to the liquid phase. (b) Initial reflectivity response of graphite at $\lambda_{probe} = 620$ nm, showing a minimal reflectivity change following excitation at $t = 0$ below melting threshold and a sharp reflectivity increase following excitation at two fluences above melting threshold.

near the solid–liquid–vapor triple point, in a form now widely, albeit approximately, accepted by many authors [7]. Such constant volume heating approximates femtosecond excitation in the limit that electron-lattice equilibration ($\tau \sim 1$ ps) occurs much more rapidly than thermal or hydrodynamic expansion ($\tau \sim 10$ ps). With available pump fluences $> 10\ \mathrm{J \cdot cm^{-2}}$, surface temperatures of several electron volts, well above the carbon melting temperature (~ 0.5 eV), are easily reached, even assuming complete electron-lattice equilibration. With constant volume heating, corresponding pressures adequate to create the liquid phase temporarily can also be reached. Slower adiabatic heating, on the other hand, stimulates sublimation directly to the vapor. Thus, in the absence of applied external pressure, femtosecond excitation is required to create the liquid phase. The closely related Column IV liquid silicon, on the other hand, can be created by either slow or ultrafast excitation. At $kT < 10$ eV (assuming $T = T_e = T_i$), $p(T)$ is determined primarily by anharmonic ionic motion and is, therefore, described by the approximate formula $p \sim 3N\gamma kT$, where γ is the Gruneisen parameter [8]. Smaller, contributions to the pressure include Thomas–Fermi electron pressure and a correction for chemical bonding, but for $kT < 10$ eV and density $\rho \sim \rho_{solid}$, the ionic contribution dominates [8]. The time scale $\tau_{release}$ for release of the pressure is estimated from the ratio of the heated depth α^{-1} to the speed of sound c_s. For graphite, $\tau_{release} \sim 10$ ps ($\alpha^{-1} \sim 5 \times 10^{-6}$ cm, $c_s \sim 5 \times 10^5\ \mathrm{cm \cdot s^{-1}}$).

3. EXPERIMENTAL RESULTS: OPTICAL PROPERTIES OF LIQUID CARBON

The experimental procedure and results on liquid carbon have been described in detail elsewhere [9–11] and are thus summarized only briefly here. Laser pulses of 90-fs duration, centered at 620-nm wavelength, and up to 0.3-mJ energy were provided by a colliding pulse mode-locked (CPM) dye laser followed by a four-stage Nd:YAG pumped optical dye amplifier system operating at 10-Hz repetition rate [12]. A beamsplitter divided the amplified pulses into pump and probe pulses, which traversed controlled and variable optical path lengths en route to the sample. The pump was focused at normal incidence onto the sample, while the probe was focused to the center of the pump spot at a range of different incidence angles. The probe pulse wavelength was varied over the range $310 < \lambda_{\text{probe}} < 700$ nm using nonlinear optical methods. Experiments were performed with samples of highly oriented pyrolytic graphite (HOPG) and type IIa diamond.

Figure 2b shows the time-resolved reflectivity response of HOPG at $\lambda_{\text{probe}} = 620$ nm following photoexcitation below and at two fluences above the melting threshold fluence $F_{\text{m}} = 0.13\ \text{J} \cdot \text{cm}^{-2}$. Below F_{m}, only slight reflectivity changes are observed, and reveal carrier dynamics in the unaltered crystalline lattice [13]. Above F_m, probe reflectivity increases sharply because of ultrafast melting of the carbon surface and the accompanying transformation of its dielectric properties and is correlated with appearance of surface damage starting at F_m. As fluence increases above F_m, the maximum reflectivity also increases slightly, showing that liquid carbon becomes slightly more reflective as it becomes hotter. In the data for $F = 1.3\ \text{J} \cdot \text{cm}^{-2}$ (and other fluences in the range $F_m < F < 2\ \text{J} \cdot \text{cm}^{-2}$), a slight partial recovery of reflectivity with time constant $\tau \sim 200$ fs is observed. This recovery corresponds closely to the carrier relaxation time observed in experiments below melting threshold [13] and is believed to correspond to equilibration of electron and lattice temperatures in the melt. Thus at $\Delta t \sim 1$ ps, the pressurized liquid is largely equilibrated and has not yet lost its optically sharp surface. In fact the approximate time interval $0.5\ \text{ps} < \Delta t < 2$ ps is a critical time window in which detailed reflectance spectroscopy can measure the dielectric properties of the pressurized, equilibrated liquid phase.

A summary of the normal incidence, reflectance spectrum of liquid carbon at $\Delta t \sim 1$ ps is presented in Fig. 3a. The open squares show $R(\Delta t \sim 1\ \text{ps})$ for $F = 2\text{J} \cdot \text{cm}^{-2}$. For reference, these data are compared to the reflectance spectrum of solid graphite and diamond and of the closely related liquid silicon. At visible wavelengths, liquid carbon is more reflective than the solid forms of carbon, but considerably less reflective

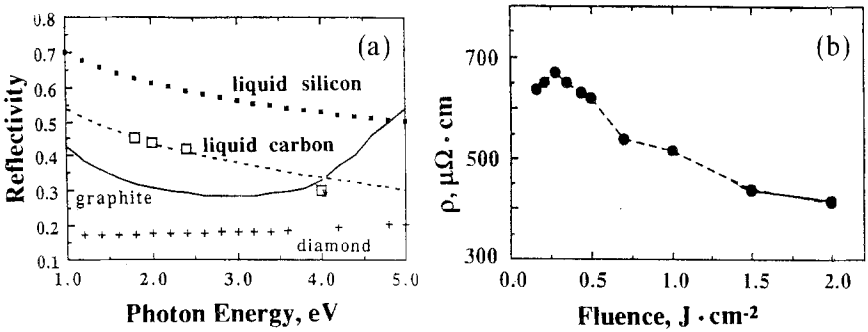

Fig. 3. (a) Normal incidence reflectance spectrum of carbon measured at $\Delta t \sim 1$ ps after a femtosecond melting pulse of 2 J · cm^{-2} (open squares); diamond (crosses); pyrolytic graphite (solid curve); liquid silicon (small filled squares). The dashed curve shows the fit of liquid carbon reflectivity to Drude dielectric function. (b) Dependence of optically determined resistivity on pump fluence.

than liquid silicon. Following the precedent for other Column IV liquid metals [14], the dashed curve represents a fit of the liquid carbon data to a Drude dielectric function of the form $\varepsilon(\omega) = 1 - \omega_p^2\tau^2/(1+\omega^2\tau^2) + i\omega_p^2\tau/\omega(1+\omega^2\tau^2)$, where ω_p is the plasma frequency and τ is an electron collision time. The same dielectric function is also consistent with, and overdetermined by, oblique incidence reflectance data described in detail elsewhere [9].

4. OPTICALLY DETERMINED ELECTRICAL RESISTIVITY OF LIQUID CARBON

From this fit we can infer a DC resistivity $\rho_C = 1/\omega_p^2\tau$, which has the value $\rho_C \sim 400\ \mu\Omega \cdot$cm for the data shown ($F = 2$ J · cm^{-2}), which correspond to heating far above the melting threshold. Just above the melting threshold, a higher resistivity, $\rho_C = 625 \pm 75\ \mu\Omega \cdot$cm, is measured. This is value agrees with a recent exploding wire measurement on a pressurized carbon rod [15] which yielded a resistivity of 700 $\mu\Omega \cdot$cm. This contrasts with lower optically determined resistivities (e.g., $\rho_{Si} \sim 80\ \mu\Omega \cdot$cm [16], $\rho_{Ge} \sim 75\ \mu\Omega \cdot$cm [17]) for other Column IV liquid metals. Thus liquid carbon can be described as a relatively poorly conducting metal.

The data in Fig. 3b show that the optically determined ρ_C *decreases* with increasing fluence, and therefore with increasing temperature, rather than increasing as in most metals. This result suggests that liquid carbon is "resistively saturated" [18]; i.e., the electron mean free path $l = v_{Fermi}\tau$ is comparable to the average interatomic spacing $N^{-1/3} \sim 2$ Å just above the melting temperature and, therefore, cannot grow any shorter with

further heating. This interpretation is supported by the value of the fitted Drude parameter $\tau \sim 1 \times 10^{-16}$ s just above F_m, which yields $1 \sim 1.7$ Å. The decrease in ρ_C with fluence suggests an approach to high-temperature plasma behavior in which resistivity is increasingly determined by Coulomb scattering and scales as $T^{-3/2}$ [19]. In addition, the conduction electron density may increase with increasing temperature, thus tending to increase ρ_C via the ω_p factor. The measured ρ_C decreases approximately as $F^{-0.6}$, suggesting that material is intermediate between "liquid" just above the melting temperature and "solid density plasma" at higher temperatures.

5. EXPERIMENTAL RESULTS: HYDRODYNAMIC SURFACE EXPANSION

Femtosecond time-resolved reflectivity at $\Delta t \gg 1$ ps can be used to measure the early stages of hydrodynamic expansion of a solid surface following heating and pressurizing by a femtosecond pump pulse. However, because the surface is no longer optically flat, analysis of the reflectivity results is more complicated. The reflectivity of an optically flat surface, depicted in Fig. 4a, is described completely by Fresnel's equations. At $\Delta t > 1$ ps, however, a surface density gradient of scale length $L \sim v_{sound} \Delta t$

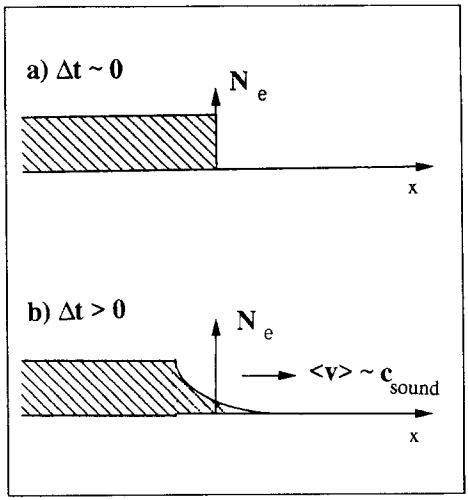

Fig. 4. (a) Electron density as a function of position for an atomically sharp solid surface. (b) Same for a hydrodynamically expanding solid surface after heating and pressurizing by a femtosecond laser pulse.

develops, as depicted in Fig. 4b, with a geometrical form given by the Riemann solution of hydrodynamic equations [20], in which $N(x) = N_0$ for $x < v_0 t$, $N(x) = N_0(3/4 - x/4v_0 t)^3$ for $-v_0 t < x < 3v_0 t$, and $N(x) = 0$ for $3v_0 t < x$. In the graded density expansion region, the dielectric function $\varepsilon(x)$ is a strong function of longitudinal distance. Consequently, reflectivity is described by the more general Helmholtz wave equations [21], which must be solved numerically at each time delay Δt.

Figure 5 presents time-resolved p-polarized reflectivity $R_p(t)$ data for (a) a free electron metal, aluminum, (b) a d-band metal; tungsten, and (c) a covalently bonded material; carbon, over a time interval $-1\,\text{ps} < \Delta t < 20\,\text{ps}$, which includes both the initial heating, melting, and equilibration ($\Delta t < 1$ ps) and the beginning stages of hydrodynamic surface expansion ($\Delta t > 1$ ps). $R_p(t)$ for Al excited at $1\,\text{J}\cdot\text{cm}^{-2}$ with $\lambda_{\text{probe}} = 620\,\text{nm}$, $\Theta_{\text{probe}} = 70°$, is shown in Fig. 5a. The reflectivity decreases with pulse width-limited fall time from an initial value of 0.80, reaching a minimum of about 0.32 in $\Delta t \sim 1$ ps, followed by a much slower partial recovery during $1\,\text{ps} < \Delta t < 15\,\text{ps}$. The most general Drude dielectric function is $\varepsilon(x, t) = \varepsilon_{10}(x) + i\varepsilon_{20}(x) - \omega_p^2\tau^2/(1+\omega^2\tau^2) + i\omega_p^2\tau/\omega(1+\omega^2\tau^2)$. For a free electron metal, however, we can safely set $\varepsilon_{10}(x) = 1$ and $\varepsilon_{20}(x) = 0$, so that the x dependence of $\varepsilon(x, t)$ in the expansion region is contained entirely in the x dependence of the atomic density $N(x)$, since ω_p^2 and τ^{-1} are proportional to $N(x)$. The data analysis is then simplified. The dotted curve in Fig. 5a was calculated based on electron heating and cooling only, *without* hydrodynamic expansion [$L(t) = 0$]. This mechanism yields a pulse width-limited fall time in $R_p(t)$ of the observed magnitude. However, an unreasonably long electron relaxation time (~ 10 ps) is required to fit the recovery. Thus a shorter more realistic recovery, derived from the solution of coupled diffusion equations [22] with electron–phonon coupling constant $3.6 \times 10^{17}\,\text{W}\cdot\text{m}^{-3}\cdot\text{K}^{-1}$ and thermal conductivity $236\,\text{W}\cdot\text{m}^{-1}\cdot\text{K}^{-1}$, is shown. On the other hand, the recovery of $R_p(t)$ is fit very well by introducing hydrodynamic surface expansion at approximately v_{sound}. The dashed curve in Fig. 5a shows the calculated $R_p(t)$ considering plasma expansion alone, *without* electron heating, at $v_{\text{exp}} = 1.2 \times 10^6\,\text{cm}\cdot\text{s}^{-1}$, close to the speed of sound. Nevertheless, this model alone cannot explain the rapid fall time of $R_p(t)$. However, when both electron heating and plasma expansion are taken into account, a very satisfying fit for Al is obtained, as shown by the solid curve in Fig. 5a. Very similar data and analysis are obtained for Ag.

$R_p(t)$ for the nonfree electron metal W are shown in Fig. 5b. The inset shows $R_p(t)$ for excitation at $0.5\,\text{J}\cdot\text{cm}^{-2}$, $\lambda_{\text{probe}} = 620\,\text{nm}$, $\Theta_{\text{probe}} = 70°$. In this case solid W simply melts into a liquid which is more reflective (0.26) than the solid (0.20), without hydrodynamic expansion. Hence the

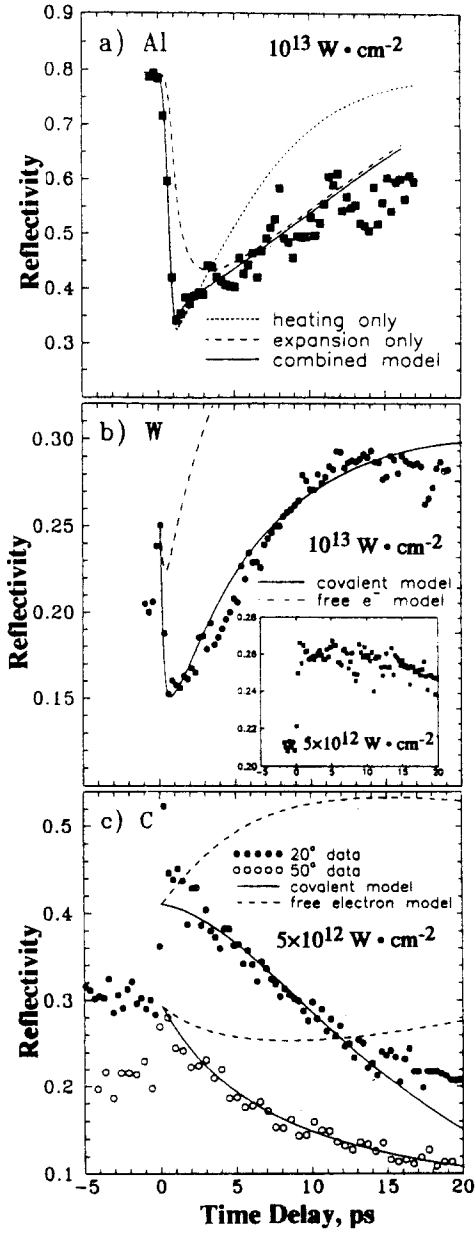

Fig. 5. Time-resolved *p*-polarized reflectivity of (a) Al, (b) W, and (c) C surfaces pump by *p*-polarized, 90-fs, 620-nm pulses at $1\,J\cdot cm^{-2}$. Curves represent theoretical models based on numerical solutions of Helmholtz wave equations, as described in the text.

liquid reflectivity persists for >10 ps. At $1\ \mathrm{J \cdot cm^{-2}}$ excitation (Fig. 5b), however, an initial reflectivity increase to the liquid value (0.26) is followed immediately by a reflectivity drop and recovery, which qualitatively resemble the pattern observed in Al and Ag. *If, however, we assume liquid W and the expanding material to be a free electron metal* [*i.e.*, $\varepsilon_{10}(x)=1$, $\varepsilon_{20}(x)=0$], *the reflectivity drop and recovery cannot be similarly explained.* The Helmholtz equations yield the dashed line, which disagrees strongly with the data. On the other hand, if we introduce $\varepsilon_{10}=11.7$ and $\varepsilon_{20}=6.7$ in the liquid, and readjust ω_p and τ to fit the initial liquid W reflectivity, the very satisfying solid curve for the W data after melting is achieved using $v_{exp}=4.6\times10^5\ \mathrm{cm \cdot s^{-1}}$. In the expansion region, $\varepsilon_{10}(x)$ and $\varepsilon_{20}(x)$ are assumed to decrease linearly with density down to the vacuum values ($\varepsilon_{10}=1$, $\varepsilon_{20}=0$). These large ε_{10} and ε_{20} values indicate a strong influence of covalency both in the liquid and the denser parts of the expansion region.

Covalency plays a similar role in the hydrodynamic expansion of carbon, as shown by $R_p(t)$ data in Fig. 5c for graphite excited at $0.5\ \mathrm{J \cdot cm^{-2}}$, with $\lambda_{probe}=620$ nm, $\Theta_{probe}=20$ and $50°$. The dashed curves show a free electron model sharply deviating from the data, while the solid curves have incorporated finite ε_{10} and ε_{20} values [23].

6. CONCLUSION

Because of their high peak intensity and short duration, femtosecond laser pulses can excite condensed matter to extremes of pressure and temperature characteristic of planetary and stellar interiors while they retain optically sharp surfaces. Moreover, quasi-equilibrium electron-ion temperatures and liquid phase molecular structure are established in as little as 1 ps following excitation, as demonstrated by the agreement described above between optical properties at 1 ps after excitation and slower time scale resistivity measurements for liquid silicon and carbon. Consequently, femtosecond laser experiments provide an important new tool for the thermophysics community. In the future, measured dielectric properties of high-temperature pressure liquids should be compared with atomic [24] and molecular dynamics [25] models. In addition, new types of time-resolved optical experiments, such as Raman scattering and X-ray scattering, can directly probe the microscopic structure of high-temperature pressure materials as well as the macroscopic dielectric properties.

ACKNOWLEDGMENTS

This research was supported by U.S. National Science Foundation Grant DMR 8858388, Robert A. Welch Foundation Grant F-1038, and Air Force Office of Scientific Research Contract F49620-89-C-0044.

REFERENCES

1. J. Squier, F. Salin, G. Mourou, and D. Harter, *Opt. Lett.* **16**:324 (1991).
2. F. G. Patterson and M. D. Perry, *J. Opt. Soc. Am. B* **8**:2384 (1991).
3. J. D. Kmetec, J. J. Macklin, and J. F. Young, *Opt. Lett.* **16**:1001 (1991).
4. H. M. Milchberg, R. R. Freeman, S. C. Davey, and R. M. More, *Phys. Rev. Lett.* **61**:2364 (1988).
5. J. C. Kieffer, P. Audebert, M. Chaker, J. P. Matte, H. Pepin, T. W. Johnston, P. Maine, D. Meyerhofer, J. Delettrez, D. Strickland, P. Bado, and G. Mourou, *Phys. Rev. Lett.* **62**:760 (1989).
6. R. Fedosejevs, R. Ottmann, R. Sigel, G. Kuhnle, S. Szatmari, and F. P. Schafer, *Phys. Rev. Lett.* **64**:1250 (1990).
7. F. P. Bundy, *Physica (Amsterdam)* **156A**:169 (1989).
8. R. M. More, K. H. Warren, D. A. Young, and G. B. Zimmerman, *Phys. Fluids* **31**:3059 (1988).
9. D. H. Reitze, H. Ahn, and M. C. Downer, *Phys. Rev. B* **45**:2677 (1992).
10. D. H. Reitze, X. Wang, H. Ahn, and M. C. Downer, *Phys. Rev. B* **40**:11986 (1989).
11. N. Bloembergen, *Nature* **356**:110 (1992).
12. W. M. Wood, G. Focht, and M. C. Downer, *Opt. Lett.* **13**:984 (1988).
13. K. Seibert, G. C. Cho, W. Kutt, H. Kurz, D. H. Reitze, J. I. Dadap, H. Ahn, M. C. Downer, and A. M. Malvezzi, *Phys. Rev. B* **42**:2842 (1990).
14. N. H. March, *Liquid Metals* (Cambridge University Press, Cambridge, 1990).
15. S. V. Lebedev and A. I. Savvatimskii, *Teplofiz. Vys. Temp. (USSR)* **24**:892 (1986); *High Temp. (USA)* **24**:671 (1986).
16. K. M. Shvarev, B. A. Baum, and P. V. Gel'd, *Fiz. Tverd. Tela (Leningrad)* **16**:3246 (1974); *Sov. Phys. Solid State* **16**:2111 (1975).
17. J. N. Hodgson, *Philos. Mag.* **6**:509 (1961).
18. N. F. Mott, *Metal-Insulator Transitions* (Taylor and Francis, London, 1974).
19. L. Spitzer, Jr., *Physics of Fully Ionized Gases* (Wiley, New York, 1962).
20. Y. B. Zeldovich and Y. P. Raizer, *Physics of Shock Waves and High Temperature Hydrodynamic Phenomena* (Academic, New York, 1966).
21. H. M. Milchberg and R. R. Freeman, *J. Opt. Soc. Am. B* **6**:1351 (1989).
22. J. G. Fujimoto, J. M. Liu, E. P. Ippen, and N. Bloembergen, *Phys. Rev. Lett.* **53**:1837 (1984).
23. X. Y. Wang and M. C. Downer, *Opt. Lett.* **17**:1450 (1992).
24. S. Kato, R. Kawakami, and K. Mima, *Phys. Rev. A* **43**:5560 (1991).
25. G. Galli, R. M. Martin, R. Car, and M. Parrinello, *Phys. Rev. B* **42**:7470 (1990).